JSR Publications

Available Online

J. Sci. Res. **15** (1), 43-53 (2023)

JOURNAL OF SCIENTIFIC RESEARCH

www.banglajol.info/index.php/JSR

Copper Doped PPy/MWCNT Nanocomposite Materials for Supercapacitor Applications

M. H. Priyadarsini[1], M. C. Adhikary[1, 2*], P. Jena[1,2], R. M. Pujahari[3]

[1]Department of Applied Physics and Ballistics, Fakir Mohan University, Balasore-756019, Odisha, India

[2]Centre of Excellence for Bioresource Management and Energy Conservation Material Development, Fakir Mohan University, Balasore-756019, Odisha, India

[3]ABES Institute of Technology, Ghaziabad-201009, Uttar Pradesh, India

Received 26 April 2022, accepted in final revised form 11 August 2022

Abstract

We report the structural, morphological, and electrochemical properties of polypyrrole (PPy), copper doped PPy (Cu/PPy), and copper doped polypyrrole multi-walled carbon nanotubes (Cu/PPy/MWCTs) prepared by oxidative polymerization technique. The incorporation of Cu in the form of nanoparticles in the composites was confirmed from XRD data. The granular morphology of PPy was observed from the FESEM micrograph. However, the size of the grains was decreased with Cu nanoparticle insertion in the matrix. The uniform distribution of Cu nanoparticles in the Cu/PPy and Cu/PPy/MWCTs nanocomposites has been evidenced from TEM images. The highest specific capacitance of 311 F/g at a scan rate of 10 mV/s is achieved in the case of Cu/PPy/MWCTs composite. It is found that the cyclic stability of these nanocomposites is enhanced due to the integration of MWCNTS and Cu nanoparticles with PPy polymer. The Cu/PPy/MWCNTs nanocomposites retained 91% of their specific capacitance even after 1000 cycles. The maximum energy density of 19.89 Wh/kg and maximum power density of 4479.71 W/kg at the scan rate of 200 mV/s were also measured for the Cu/PPy/MWCNTs nanocomposite. Our study thus indicates that the prepared Cu/PPy/MWCTs nanocomposite could be a potential candidate for application in supercapacitor and hybrid type storing devices.

Keywords: Nanocomposite; Polypyrrole; MWCNT; Copper; Capacitance; Supercapacitor.

doi: http://dx.doi.org/10.3329/jsr.v15i1.59397 J. Sci. Res. **15** (1), 43-53 (2023)

1. Introduction

The present-day energy research is oriented toward the development of alternative energy storage resources. Alternative energy storage resources such as batteries and supercapacitors are the most promising electrochemically energy storage devices [1,2]. Though lithium-ion batteries have received enormous favor in terms of compact size and high energy density, the major problem is its slow charging-discharging cycle, low power density, and degradation of the active materials with continuous cycling [3,4]. Unlike the

* *Corresponding author*: mcadhikary@gmail.com

Lithium-ion battery, the energy in the capacitor is stored electro-statically. Supercapacitors are considered to be the energy storage system having the hybrid properties of conventional batteries as well as capacitors [5,6]. It exhibits a high capacity and long cycle life without the involvement of the chemical reaction. Also, supercapacitors form a bridge between the two conventional energy storage systems in terms of both high energy density and high capacity. It can be cycled up to many times [7,8]. Based on different charge storage mechanisms, supercapacitors are of two types: electric double-layer capacitors and pseudo-capacitor or redox supercapacitors. In the case of an electric double-layer capacitor, the accumulation of energy is done through the separation of electronic and ionic charges at the electrode-electrolyte interface. But in the case of Pseudo-capacitor or redox supercapacitor; it is based on redox-active electrode materials such as metal oxides and conducting polymers. Here, the accumulation of charge is done on the reversible surface through faradaic reactions. However, there is still a challenging task to develop pseudo-capacitive electrode materials for designing high-energy-density devices [9-11].

In context to this, conducting polymers such as polypyrrole (PPy), polyaniline (PANI), and poly (3, 4-ethylenedioxy thiophene) (PEDOT) and their derivatives attracted much more attention to researchers. In recent years, it is investigated as electrode materials for supercapacitors due to their unique properties such as high charge density, high doping–doping rates in charge-discharge processes, and simple synthesis via chemical or electrochemical methods [12-15]. Also, carbon nanotubes (CNTs), both single- and multiwall structures have been explored as a potential candidate for energy storage and conversion devices, due to their outstanding physical and chemical properties [16-21]. The incorporation of MWCNTs into the polymeric matrices increases the specific surface area, which enhances the electrical conductivity and mechanical strength as a result the electrochemical properties increase of these composite materials [16-25]. Further, the conducting polymer-metal nanocomposites form a potential class of electrode materials [26,27]. When the transition metals (Ni, Co, Fe, Mn, Cu, etc.) were doped in conducting polymers, the dopant ions act as redox-active catalysts and improve the capacitance leads an increase in energy density [28,29].

Although PPy/MWCNTs-based nanocomposite electrode materials have been investigated extensively for high electrochemical performance by employing various synthesis methods [18,21-24]. However, some of the literature reports are available on the electrochemical properties of copper chloride as well as oxide materials and its composites [25,30]. To the best of our knowledge, none of the literature reports available on the investigation of electrochemical properties of Cu nanoparticles doped PPy/MWCNTs nanocomposites. In this present study, in-situ oxidative polymerization techniques were used for the synthesis of Cu/PPy, and Cu/PPy/MWCNTs nanocomposites. The structural characterization, phase purity, and morphology of prepared materials were carried out by XRD, FTIR, Raman spectroscopy, FE-SEM, and TEM. Further, the electrochemical performances of the prepared samples were studied for supercapacitor applications.

2. Experimental

2.1. *Synthesis of PPy*

The chemical oxidative polymerization technique was used for the synthesis of PPy, in which $(NH_4)_2S_2O_8$ (Ammonium Persulphate APS) was employed as an oxidant. 1.0 mL of pyrrole monomer was dissolved in 70 mL of 1.5 M HCl solution. Separately, 2.04 g of $(NH_4)_2S_2O_8$ has been dissolved in 20 mL of de-ionized water in a beaker and then dropwise added to the previously prepared solution. Then it was stirred continuously with a constant speed for 5 h at ambient temperature. The precipitate was washed with ethanol as well as de-ionized water repeatedly and dried in a hot air oven at 60 ºC for 12 h.

2.2. *Synthesis of nanocomposites*

The Cu/PPy, and Cu/PPy/MWCNTs nanocomposites were prepared by the same in-situ oxidative polymerization technique and its schematic diagram is shown in Fig. 1. 65 mg of MWCNTs and 1.24 g of acetyl-tri-methyl-ammonium bromide were mixed in 150 mL of 1.5 M HCl solution and sonicated for 45 min. in ambient temperature. Separately, 1.25 mL of pyrrole monomer was mixed with 50 mL of 1.5 M HCl solution. Then, Cu nitrate solution of 2.5 wt% has been poured gradually into the above-mentioned pyrrole solution and continuously stirred for 15 min. at ambient temperature. In the next step, the prepared Cu nitrate- pyrrole solution was added to the prepared suspension of MWCNTs. Similar to the previous process, 74 mL solution of 1.5 M HCl and 2.04 g of $(NH_4)_2S_2O_8$ dissolved in 20 mL of de-ionized water was then added dropwise to the bulk solution of 70 mL. Cu-nitrate doped pyrrole containing MWCNTs continuously stirred for 5 h in ambient conditions. The same was kept at a low temperature of about 1–5 °C for 12 h for polymerization. Then, the precipitate was filtered and washed with distilled water and ethanol several times and vacuum-dried at 70 °C for 12 h to get the Cu ion doped PPy – MWCNTs nanocomposite.

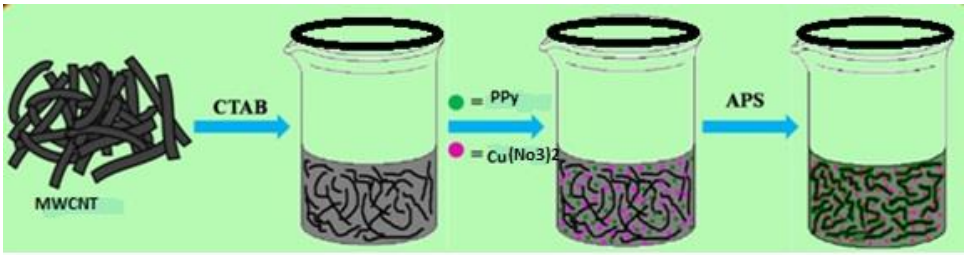

Fig. 1. Schematic diagram of Cu/PPy, and Cu/PPy/MWCNT nanocomposites preparation.

2.3. *Measurement techniques*

The X-ray diffraction (XRD) patterns were recorded by using X'pert-PRO MPD, PANalytical diffractometer using Cu Kα radiation (λ = 1.5406 Å), ranging from 10º to 80º

with step size 0.02. The morphology of the prepared samples was analyzed by FESEM (Carl Zeiss-SUPRA 40) and HR-TEM (JEOL 2100). The FTIR spectra of the samples were recorded by using a Thermo NICOLET 6700 spectrometer in the range of 4000 to 400 cm^{-1}. The Raman spectra were recorded using RAMNOR HG-2S spectrometer (Jobin-Yvon, France) by an argon ion laser with 10 mW power.

The current-voltage measurements of the prepared samples were recorded by using a Keithley 2400 source meter at room temperature with a scan rate of 0.1 V/s. The electrochemical characterizations were carried out by a potentiostatic electrochemical workstation (Biologic SP-150 VMP-3) at room temperature.

The energy densities of the prepared samples were calculated by the following equation: Energy density (E) = $1/2(CV^2)$

Where C is the specific capacitance in F g^{-1}, and V is the operating voltage, while power densities were calculated by the following equation: Power density (P) = E/t
Where t is the time in second for a complete cycle. Hence by using these formulas we have calculated the energy density and power density of the prepared samples.

3. Result and Discussion

3.1. *X-ray diffraction analysis*

The XRD patterns of prepared pure PPy, Cu/PPy, and Cu/PPy/MWCNT nanocomposite samples were depicted in Fig. 2. For the Cu/PPy/MWCNT sample, the appearance of the XRD peaks at 2θ values of 38.05, 42.28, and 73.38º corresponds to the face-centered cubic phase of the Copper (Cu) atom patterns (111), (220), and (311) respectively. Also, the same patterns were observed for the Cu/PPy sample. The appearance of intense peaks in Cu/PPy and Cu/PPy/MWCNTs nanocomposite samples indicates the crystalline nature due to the existence of Cu nanoparticles. Further, a broad peak was observed within the 2θ range ~ 17-30º for all the XRD patterns, which is due to the amorphous phase of PPy.

3.2. *FE-SEM analysis*

The morphology of PPy, Cu/PPy, and Cu/PPy/MWCNT composites are investigated with the help of FE-SEM. The pure polymer PPy suggested the granular morphology (Fig. 3a) of bigger size; while Cu ion doped PPy is granular with a comparatively smaller size than pure PPy as shown in Fig. 3b. The Cu/PPy coated MWCNTs were shown in Fig. 3c which are a little bit non-uniform. The non-uniformity in the coating may be attributed to the presence of the van der Waals forces between MWCNTs and the interaction between Cu/PPy and MWCNTs.

3.3. TEM analysis

The high-resolution TEM images of Cu/PPy and Cu/PPy/MWCNT composites are shown in Figs. 4 (a) and (b) respectively. From Fig. 4a, it is found that the copper nanoparticles

are uniformly distributed into the PPy polymer matrix except in certain regions where the agglomerated form of PPy is also seen. Fig. 4b suggests a less uniform coating of Cu/PPy onto MWCNTs.

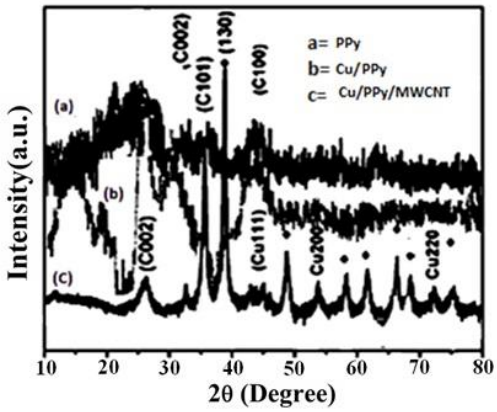

Fig. 2. XRD patterns of the (a) PPy, (b) Cu/PPy, and (c) Cu/PPy/MWCNTs samples.

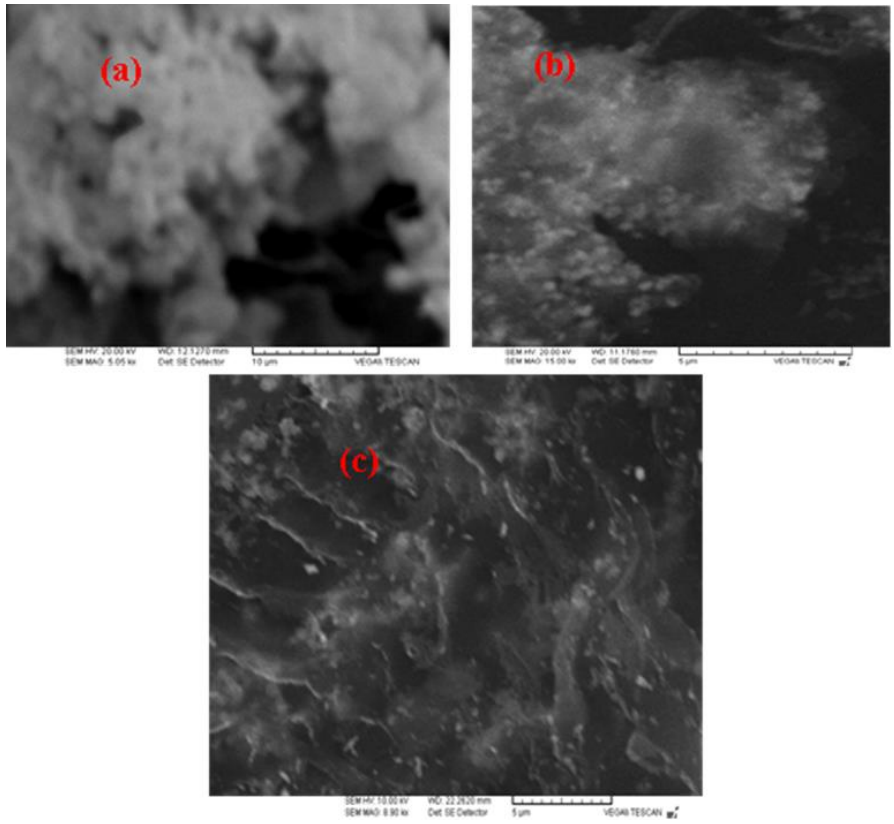

Fig. 3. FE-SEM images of the prepared (a) pure PPy, (b) Cu/PPy, and (c) Cu/PPy/MWCNT nanocomposite samples.

3.4. *FTIR spectra analysis*

The FTIR spectra were recorded for PPy, Cu/PPy, and Cu/PPy/MWCNTs nanocomposite samples are shown in Fig. 5. For all three samples, a broad absorption band is observed at around 3398 cm^{-1}, which is the signature of stretching vibrations N-H bond. The band at 3102 cm^{-1} corresponds to stretching vibrations of the aromatic C-H bonds. The observed peaks at around 1557 and 1473 cm^{-1} were the characteristic bands in PPy and correspond to the vibrations of the ring structure of pyrrole. The characteristic bands at 1308 and 1011 cm^{-1} were corresponds to in-plan deformation of =C–H, and at 924 cm^{-1} attributed to the out-of-plan =C–H modes of vibration. The observed band at 1198 cm^{-1} was attributed to stretching vibrations of C-N bonds. From FTIR spectra, it has been observed that the bands at 1557, 1473, and 1198 cm^{-1} of PPy shifted gradually to 1560, 1478, and 1204 cm^{-1}, respectively. Further, these characteristics bands of the PPy changed to 1569, 1488, and 1244 cm^{-1}, respectively in Cu/PPy/MWCNT. This fascinating occurrence may be due to the interaction of Cu nanoparticles with the Cu/PPy and Cu/PPy/MWCNT nanocomposites.

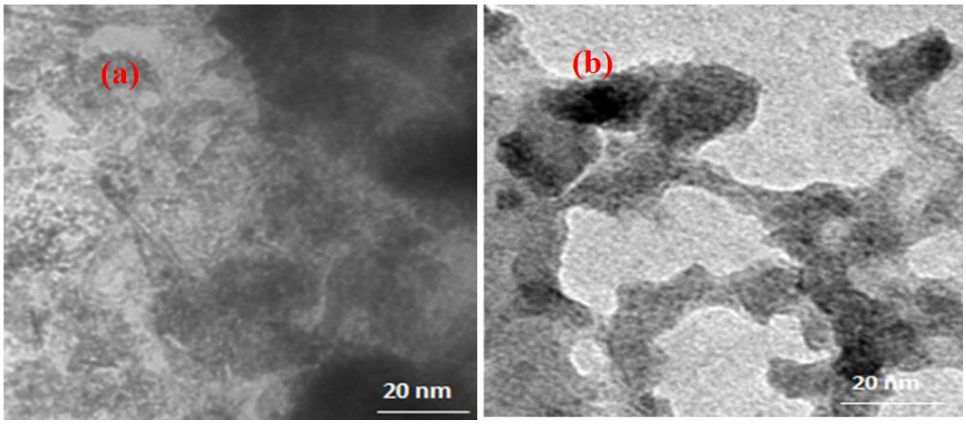

Fig. 4. TEM images of the prepared (a) Cu/PPy and (b) Cu/PPy/MWCNT nanocomposite samples.

3.5. Raman spectra analysis

Fig. 6. showed the Raman spectra of PPy, Cu/PPy, and Cu/PPy/MWCNTs nanocomposites. The observed peaks at 1368 and 1580 cm^{-1} in the pure PPy spectrum are due to the stretching of the ring structure as well as backbone modes C=C vibrations, respectively [24]. The band appears at 1378 cm^{-1} and is attributed to the in-plan deformation of the C–H bond. Further, two very small bands at 980 and 920 cm^{-1} are ascribed to the polaronic and bipolaronic structure, respectively. For Cu/PPy composite, the observed Raman band at 1579 cm^{-1} is attributed to backbone C=C stretching as well as the G band of Cu. Further, the Raman band at 1371 cm^{-1} is attributed to the D band of Cu-C. However, in Cu/PPy/MWCNT nanocomposite sample the observed Raman D and G

bands at 1370 and 1600 cm^{-1}, respectively, are slightly shifted. This shifting of Raman bands is attributed to the π-π interactions of Cu-PPy.

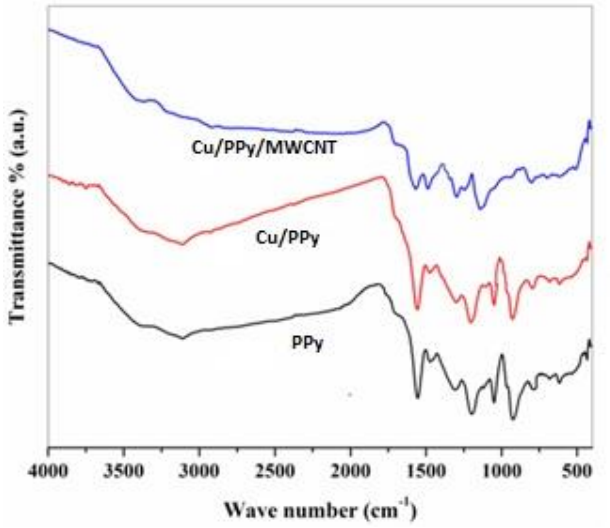

Fig. 5. FTIR spectra of PPy, Cu/PPy, and Cu/ PPy/ MWCNT nanocomposite samples.

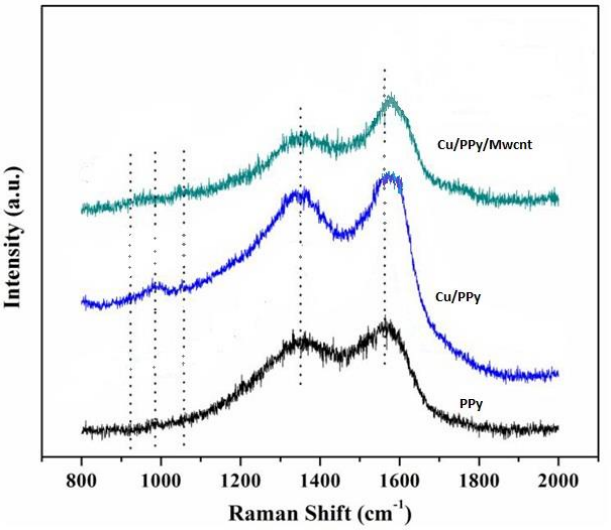

Fig. 6. Raman spectra of the prepared pure PPy, Cu/PPy, and Cu/PPy/MWCNT nanocomposite samples.

3.6. *Electrochemical measurements*

Specific capacitance versus current density plots for all three samples is shown in Fig. 7a. From the plot, it is found that the specific capacitance decreases with an increase in

current density for all the three prepared electrode materials. This behavior of decrease of specific capacitance at high current densities may be attributed to the sluggish electrochemical reactions that occurred at the electrode at that higher current densities. Further for all the prepared electrode materials, the specific capacitance was also derived from charge-discharge values. It is seen that Cu/PPy/MWCNT nanocomposite exhibits a higher specific capacitance of 480 F/g at a current density of 0.5 A/g. However, the specific capacitance of Cu/PPy and pure PPy are found to be 400 and 240 F/g, respectively, with the same current density.

The electrode materials and their cyclic stabilities were examined up to 1000 successive charge-discharge cycles at a constant scan rate of 10 mV/s. Specific capacitance vs. cycles number plots for PPy, Cu/PPy, and Cu/PPy/MWCNT nanocomposites were depicted in Fig. 7b. The Cu/PPy/MWCNTs nanocomposite retained its 91% of specific capacitance even after 1000 successive cycles. Whereas, pure PPy and Cu/PPy retained their 76 %, and 78 % of specific capacitance after 1000 cycles, respectively. The existence of Cu nanoparticles as well as PPy nanocomposites may be the reasons for enhanced cycle stability [31]. The obtained specific capacitance values of all the prepared electrode materials at different current densities are shown in Table 1. The energy densities and power densities of all the electrode materials at different current densities are also calculated and presented in Table 2 and Table 3. The obtained highest energy density of 19.89 Wh/kg and power density of 4479.71 W/kg at the scan rate of 200 mV/s of the Cu/PPy/MWCNT composite may be due to the existence of Cu nanoparticles. From Table 2 and Table 3, it has been observed that the power density increases with a decrease in energy density values.

Further, Fig. 8 shows the I–V characteristics of the pure PPy, Cu/PPy, and Cu/PPy/MWCNT nanocomposites. At room temperature, the I–V characteristics were studied within the potential range of –4 to 4 V. It has been observed that with an increase in applied voltage the current also increases nonlinearly for all the electrode materials. This nonlinearity in I–V curves indicated the rectifying nature of performance.

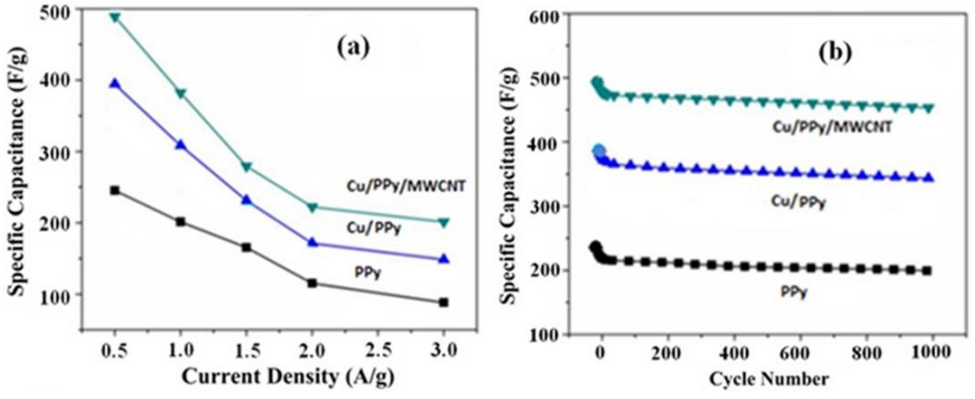

Fig. 7. (a) Specific capacitance (F/g) vs current density (A/g) (b) Specific capacitance (F/g) vs cycle number of the prepared PPy, Cu/PPy, and Cu/PPy/MWCNT nanocomposite samples.

Table 1. Specific capacitance (F/g) values of the pure PPy, Cu/PPy, and Cu/PPy/MWCNT nanocomposite samples with various scan rates.

Name of Sample	10 mV/s	20 mV/s	50 mV/s	100 mV/s	200 mV/s
PPy	180	121	63	47	31
Cu/PPy	212	137	76	59	52
Cu/PPy/MWCNT	311	218	111	64	55

Table 2. Energy density (W h/kg) values of the pure PPy, Cu/ PPy, and Cu/ PPy /MWCNT nanocomposite samples with various scan rates.

Sample	10 mV/s	20 mV/s	50 mV/s	100 mV/s	200 mV/s
PPy	63.34	42.36	21.74	16.05	10.36
Cu/PPy	75.70	49.03	27.33	21.31	18.81
Cu/PPy/MWCNT	110.90	77.82	39.78	23.08	19.89

Table 3. Power density (W/kg) values of the pure PPy, Cu/PPy, and Cu/PPy/MWCNT nanocomposite samples with various scan rates.

Sample	10 mV/s	20 mV/s	50 mV/s	100 mV/s	200 mV/s
PPy	723.91	975.79	1279.65	1919.22	2558.22
Cu/PPy	815.93	1103.90	1533.89	2399.59	4293.54
Cu/PPy/MWCNT	1247.93	1751..81	2239.83	2599.83	4479.71

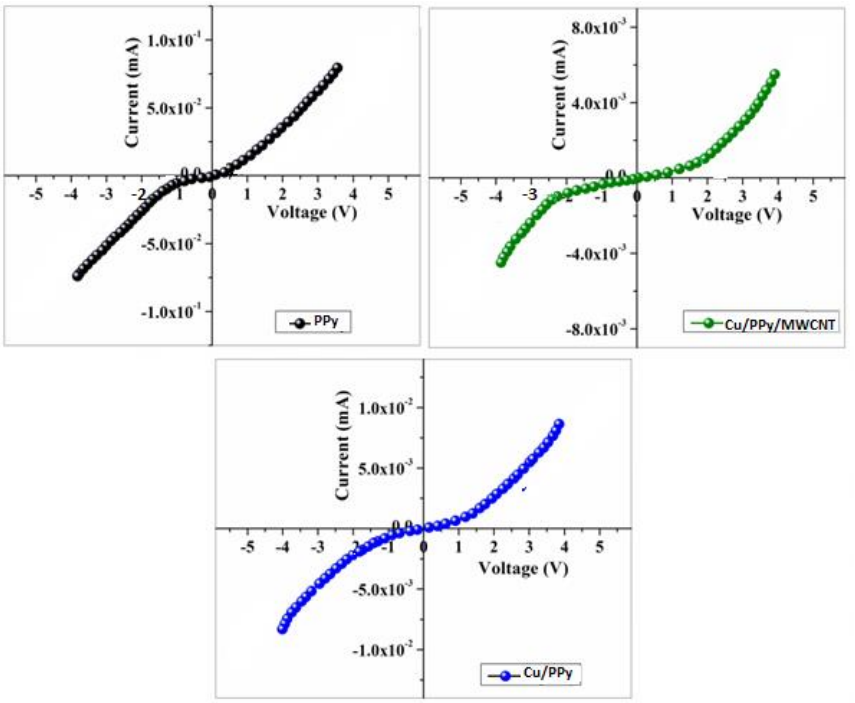

Fig. 8. I –V Characteristics of pure PPy, Cu/PPy, and Cu/PPy/MWCNT nanocomposite samples.

4. Conclusion

Pure PPy, Cu/PPy, and Cu/PPy/MWCNT nanocomposites were successfully prepared by the *in situ* polarization method. FESEM images showed that the granular nature of PPy and its grain size decreased with Cu nanoparticle composites. TEM images showed the uniform distribution of Cu ions. XRD analysis confirmed the formation of Cu nanoparticles on the MWCNTs. Electrochemical characterization showed the highest specific capacitances for the nanocomposite of Cu/PPy/MWCNT as compared to Cu/PPy nanocomposite. The maximum energy density of 19.89 Wh/kg and the maximum power density of 4479.71 W/kg at the scan rate of 200 mV/s were achieved for Cu/PPy/MWCNT nanocomposite. Also, the nanocomposite Cu/PPy/MWCNTs electrode materials exhibited high cyclic stability with 91 % specific capacitance retention after 1000 cycles. Hence, the prepared Cu/PPy/MWCTs nanocomposite material could be a potential candidate for supercapacitor applications.

Acknowledgments

We gratefully acknowledge the Odisha Higher Education Program for Excellence and Equity (OHEPEE), Higher Education Department, Government of Odisha, INDIA, assisted by the World Bank for financial support.

References

1. M. Winter and R. J. Brodd, Chem. Rev. **104**, 4245 (2004). https://doi.org/10.1021/cr020730k
2. M. A. L. Reddy, S. R. Gowda, M. M. Shaijumon, and P. M. Ajayan, Adv. Mater. **24**, 5045 (2012). https://doi.org/10.1002/adma.201104502
3. J. P. Pender, R. M. Penner, and C. B. Mullins, ACS Nano **14**, 1243 (2020). https://doi.org/10.1021/acsnano.9b04365
4. S. Chen, F. Dai, and M. Cai, ACS Energy Lett. **5**, 3140 (2020). https://doi.org/10.1021/acsenergylett.0c01545
5. A. Burke, J. Power Sources **91**, 37 (2000). https://doi.org/10.1016/S0378-7753(00)00485-7
6. P. Simon and Y. Gogotsi, Nature Mater. **7**, 845 (2008). https://doi.org/10.1038/nmat2297
7. D. Ghosh, S. Giri, S. Kalra, and C. K. Das, J. Appl. Sci. **2**, 70 (2012). https://doi.org/10.4236/ojapps.2012.22009
8. M. C. Adhikary, M. H. Priyadarsini, S. K. Rath, and C. K. Das, J. Nanoparticle Res. **19**, 314 (2017). https://doi.org/10.1007/s11051-017-4008-2
9. M. S. Balogun, W. Qiu, W. Wang, P. Fang, X. Lu, and Y. Tong, J. Mater. Chem. A **3**, 1364 (2015). https://doi.org/10.1039/C4TA05565A
10. M. A. A. Moh Abdah, N. H. N. Azaman, S. Kulandaivalu, and Y. Sulaiman, Mater. Design **186**, ID 108199 (2020). https://doi.org/10.1016/j.matdes.2019.108199
11. J. Sun, C. Wu, X. Sun, H. Hu, G. Zhi, L. Hou, and C. Yuan, J. Mater. Chem. A **5**, 9443 (2017). https://doi.org/10.1039/C7TA00932A
12. Q. Wang, J. J. Li., F. Gao, W. S. Li, K. Wu, and X. Wang, New Carbon Mater. **23**, 275 (2008). https://doi.org/10.1016/S1872-5805(08)60030-X
13. K. A. Noh, D. W. Kim, C. S. Jin, K. H. Shin, J. H. Kim, and J. M. Ko, J. Power Sources **124**, 593 (2003). https://doi.org/10.1016/S0378-7753(03)00813-9
14. J. H. Park, J. M. Ko, O. O. Park, and D. W. Kim, J. Power Sources **105**, 20 (2002). https://doi.org/10.1016/S0378-7753(01)00915-6

15. M. Noked, S. Okashy, T. Zimrin, and D. Aurbach, Angewandte Communicat. **51**, 1568 (2012). https://doi.org/10.1002/anie.201104334
16. M. M. Rahaman, D. R. Sarker, M. M.Rahman, and M. O. Faruk, J. Sci. Res. **13**, 243 (2021). https://doi.org/10.3329/jsr.v13i1.48356
17. D. N. Futaba, K. Hata, T. Yamada, T. Hiraoka, Y. Hayamizu, Y. Kakudate, O. Tanaike, H. Hatori, M. Yumura, and S. Iijima, Nature Mater. **5**, 987 (2006). https://doi.org/10.1038/nmat1782
18. X. Lin and Y. Xu, Electrochemica Acta **53**, 4990 (2008). https://doi.org/10.1016/j.electacta.2008.02.020
19. T. Chen and L. Dai, Mater. Today **16**, 272 (2013). https://doi.org/10.1016/j.mattod.2013.07.002
20. A. Afzal, A. F. Abuillaiwi, A. Habib, M. Awais, B. S. Waje, and A. M. Atieh, J. Power Sources **352**, 174 (2017). https://doi.org/10.1016/j.jpowsour.2017.03.128
21. A. Imani, G. Farzi, and A. L. Taief, Int. Nano Lett. **3,** 52 (2013). https://doi.org/10.1186/2228-5326-3-52
22. C. Du, J. Yeh, and N. Pan, Nanotechnology **16**, 350 (2005). https://doi.org/10.1088/0957-4484/16/4/003
23. M. Hughes, M. S. P. Shaffer, A. C. Renouf, C. Singh, G. Z. Chen, J. Fray, and A. H. Windle, Adv. Mater. **14,** 382 (2004). https://doi.org/10.1002/1521-4095(20020304)14:5<382::AID-ADMA382>3.0.CO;2-Y
24. S. Dhibar and C. K. Das, J. Appl. Polym. Sci. **130,** 554 (2013). https://doi.org/10.1002/app.39176
25. V. V. Kondratiev, V. V. Malev, and S. N. Eliseeva, Russian Chem. Rev. **85**, 14 (2016). https://doi.org/10.1070/RCR4509
26. M. E. Rhazi, S. Majid, M. Elbasri, F. F. Salih, L. Oularbi, and K. Lafdi, Int. Nano Lett. **8**, 79 (2018). https://doi.org/10.1007/s40089-018-0238-2
27. M. Cui and X. Meng, Nanoscale Adv. 2, 5516 (2020). https://doi.org/10.1039/D0NA00573H
28. V. Augustyn, P. Simon, and B. Dunn, Energy Environ. Sci. **7**, 1597 (2014). https://doi.org/10.1039/c3ee44164d
29. A. S. Patil, M. D. Patil, G. M. Lohar, G. M. Jadhav, and J. V. Fulari, Ionics **23**, 1259 (2017). https://doi.org/10.1007/s11581-016-1921-9
30. B. Prusty, M. C. Adhikary, and C. K. Das, Chem. Sci. Int. J. **6**, 91 (2015). https://doi.org/10.9734/ACSJ/2015/15866
31. C. K. Das, B. Prusty, M. C. Adhikary, and S. Kalra, Int. J. Eng. Sci. Res. Tech. **4**, 324 (2015).